Dalton Transactions

A water-soluble cyclometalated Iridium(III) complex for pH sensing based on aggregation-induced enhanced phosphorescence

Journal:	*Dalton Transactions*
Manuscript ID	DT-ART-12-2018-004861.R2
Article Type:	Paper
Date Submitted by the Author:	25-Feb-2019
Complete List of Authors:	Ohno, Keiji; epartment of Chemistry, Graduate School of Science and Engineering, Saitama University Sakata, Tetuya; a. Department of Chemistry, Graduate School of Science and Engineering, Saitama University Shiiba, Machi; Ochanomizu University Senior High School Nagasawa, Akira; Saitama University, Department of Chemistry, Graduate School of Science and Engineering Fujihara, Takashi; Saitama University, Comprehensive Analysis Center for Science

Journal Name

ARTICLE

A water-soluble cyclometalated Iridium(III) complex for pH sensing based on aggregation-induced enhanced phosphorescence

Received 00th January 20xx,
Accepted 00th January 20xx

DOI: 10.1039/x0xx00000x

www.rsc.org/

Keiji Ohno,[a] Tetuya Sakata,[a] Machi Shiiba,[b] Akira Nagasawa,[a] and Takashi Fujihara[c*]

The novel water-soluble monoanionic Ir(III) complex Na[Ir(ppy)$_2$(SB-COO)] (**2**; Hppy = phenylpyridine; HSB-COOH = 4-carboxylanilinesalicylaldehyde Schiff base), which was obtained by the reaction of the novel Ir(III) complex [Ir(ppy)$_2$(SB-COOH)] (**1**) with NaOEt, in its aqueous solution showed hydrogen ion (H^+)-responsive aggregation-induced enhanced phosphorescence (AIEP). Both of these complexes exhibited very weak and relatively strong emissions in solution and solid states, respectively. The pH-responsiveness of **2** was evaluated from its emission spectra in aqueous solution in the pH range of 8.7–1.8. Above pH 6, **2** showed weak emission with a maximum at 508 nm. Upon decreasing the pH to 4.7, AIEP with a bathochromic shift to 618 nm was induced by aggregation of **1**, whereby the intensity at 618 nm was increased approximately by 50-fold compared to that at pH 6.0. This enhancement is due to restrictions of the geometrical changes in the six-membered chelate ring of the ancillary ligand (Ir–N–C–C–C–O–) and of intramolecular rotations in the excited state. The enhanced luminescence originates from spin-forbidden metal-to-ligand-ligand charge transfer (^{3}MLLCT). Below pH 2.8, the emission intensity decreases owing to the decrease in the population of emissive complex **1** upon dissociation of the ancillary ligand from the Ir(ppy)$_2$ unit.

Introduction

The luminescent properties of cyclometalated iridium(III) complexes in solid and solution states have been widely investigated,[1,2,3] and the combination of cyclometalating ligands and ancillary ligands as emitting and functional sites, respectively, is of considerable importance in the development of luminescent devices[1] as well as chemical-[2] and bio-sensors[3]. Most Ir complexes show weak emissions in the solid state compared to those in diluted solutions because of the enhanced nonradiative decay due to strong intermolecular interactions in the solid state.[4] This kind of behavior is termed as aggregation-caused quenching (ACQ), and it is one of the issues that must be addressed for appropriate applications of the complexes in luminescent devices and sensors.

The opposite situation (anti ACQ), i.e., enhanced emission in the aggregated and solid states compared to that in a diluted solution, has been accomplished.[5] The phenomenon is called aggregation-induced enhanced phosphorescence (AIEP), aggregation-induced phosphorescent emission (AIPE), aggregation-induced enhanced emission (AIEE), or enhanced phosphorescence emission in the solid state (EPESS).[5] The enhancement in emission originates from various factors of the excited state, such as restriction of intramolecular rotations,[6] constraint of chelate ring distortions,[7] and the formation of excimers upon π–π stacking of adjacent pyridyl rings in ppy ligands.[8] When organic compounds or complexes with bulky rotatable moieties are dissolved into solution, vibrational deactivation owing to intramolecular rotations causes largely weakened or even fully quenched emissions. In the aggregated state, these rotations can be restricted; thus, enhancing emission intensity. Upon excitation of complexes containing six-membered chelate ring, i.e., those formed by the ancillary ligand and the metal center, in solution, significant geometrical changes in the chelating moiety can arise. Conversely, in the solid state, ligand distortions are usually restricted. Accordingly, emission is enhanced.

The study of luminescent pH-sensing materials is gaining importance in the fields of environmental and biological chemistry,[9] and various principles, such as excited-state intramolecular proton transfer (ESIPT) and photo-induced electron transfer (PET), have been explored in the development of such materials. Recently, organic compounds bearing pH-sensitive functional groups have been applied to pH monitoring based on AIEE in chemical solution and living cells.[10] In the case of Ir complexes, emission color switching based on electronic state changes at emitting sites upon

[a] Department of Chemistry, Graduate School of Science and Engineering, Saitama University, 255 Shimo-Okubo, Sakura-ku, Saitama 338-8570, Japan.
[b] Ochanomizu University Senior High School, 2-1-1 Ohtsuka, Bunkyo-ku, Tokyo 112-8610, Japan.
[c] Comprehensive Analysis Center for Science, Saitama University, 255 Shimo-Okubo, Sakura-ku, Saitama 338-8570, Japan.

† Electronic Supplementary Information (ESI) available: Detail of theoretical calculations for **1** and **2** in the ground and excited states and emission and excitation spectra of **1** and **2**.

protonation and deprotonation have been studied.[5h,11] However, pH-dependent AIEP in such complexes has not been investigated much. In fact, to the best of our knowledge, only one report on pH-responsive AIEP by Ir complex has been published.[12] AIEP triggered by changes in pH is an effective strategy for further development of Ir complexes, because unlike phosphorescence in solution, AIEP is not susceptible to O_2 molecules. Furthermore, the dissolution of Ir complexes into aqueous solutions would be appropriate for applications in sensors under various conditions.[13,5i] However, the sensing properties of Ir complexes are usually studied in organic solvents owing to their poor water solubilities.

In this work, we present the novel water-soluble anionic Ir complex Na[Ir(ppy)$_2$(SB-COO)] (**2**; ppy$^-$ = phenylpyridinate; HSB-COOH = 4-carboxylanilinesalicylaldehyde Schiff base;[14] Fig. 1), which was obtained by a deprotonation of the novel neutral complex [Ir(ppy)$_2$(SB-COOH)] (**1**) and exhibits hydrogen ion (H$^+$)-responsive AIPE. The luminescent properties of both complexes in solution and the solid states are also presented and discussed.

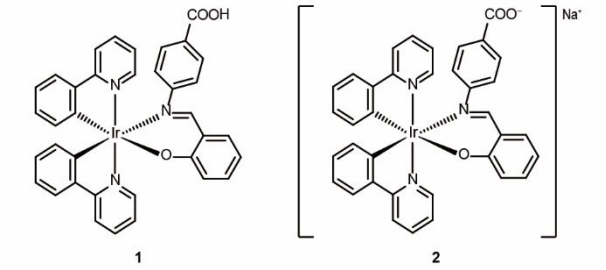

Fig. 1. Structures of the protonated neutral Ir(III) complex [Ir(ppy)$_2$(SB-COOH)] (1) and deprotonated anionic Ir(III) complex Na[Ir(ppy)$_2$(SB-COO)] (2).

Results and Discussion

Syntheses and characterizations

Complex **1** was obtained as an orange powder by the reaction of the precursor Ir dimer [{Ir(ppy)$_2$}$_2$(μ-Cl)$_2$][15] with HSB-COOH in the presence of NEt$_3$ in MeOH.[6a] Complex **1** was found to be soluble in acetone, THF, and DMSO but not in MeOH and H_2O. The reaction of **1** with 1 equivalent of NaOMe in MeOH afforded **2**, which was found to be soluble in H_2O, MeOH, and DMSO.

The integral intensities of the relevant signals in the ^{1}H NMR spectra of **1** and **2** recorded in DMSO-d_6 revealed that the ppy$^-$ and corresponding ancillary ligand are present in the complexes in a 2:1 ratio. Resonance of the –COO*H* proton of **1** is detected at δ = 12.7, indicating a protonated complex with neutral charge. As expected, no signal for the –COO*H* proton is observed in the spectrum of **2**, indicating a monoanionic complex.

As shown in Fig. 2, the UV-Vis absorption spectra recorded in DMSO present broad bands in the visible region. The absorption maxima of **1** and **2** are observed at 406 and 404 nm, respectively, and the bands tail to ca. 500 nm. The wide broad bands are assigned to a combination of metal-to-ligand charge transfer (MLCT), in which electron transfers from a metal d orbital to vacant π* orbitals on ppy$^-$ and SB-COO(H) ligands, i.e., mixed transitions of ML$_{ppy}$CT and ML$_{SB\text{-}COO(H)}$CT, as well as ligand centered π-π* transitions (LC) and intraligand charge transfer (ILCT) by the ancillary ligands. These assignments are supported by time-dependent density functional theory (TD-DFT) study (*vide infra*).

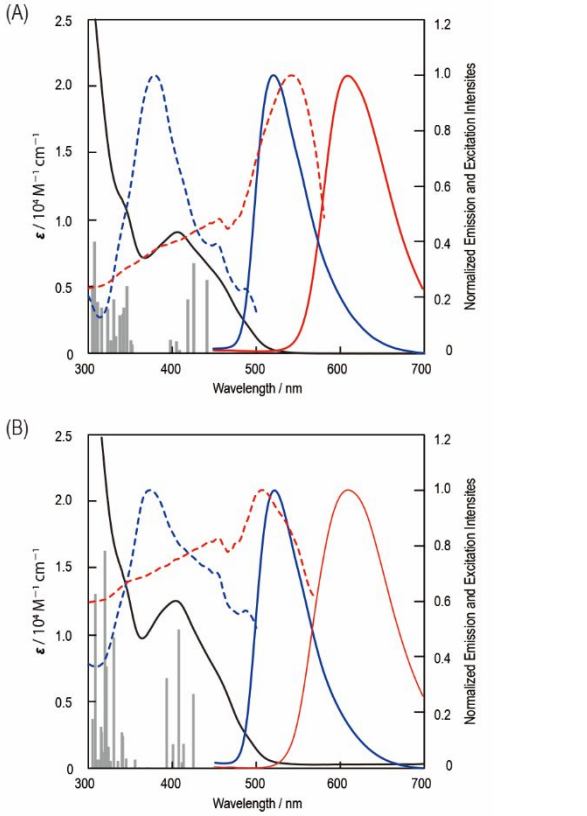

Fig. 2. Absorption and emission (λ_{ex} = 365 nm) spectra and results of time-dependent density functional theory (TD-DFT) for **1** (A) and **2** (B) (solid black and blue lines: UV-Vis absorption and emission spectra in DMSO, respectively; solid red line: emission spectra in the solid state; dashed blue and red lines: excitation spectra in DMSO and solid state, respectively; gray bars: calculated transition models).

The complexes in degassed DMSO exhibit a very weak green emission upon excitation at 365 nm. The emission spectra of **1** and **2** present emission bands with maxima at 518 and 522 nm, respectively (Fig. 2), and their quantum yields are 0.005. The emission lifetimes are 0.63 and 1.13 μs for **1** and **2**, respectively, which indicate the phosphorescent character of their emissions. The emissions most likely originate from ^{3}ML$_{ppy}$CT character, and the low emission quantum yields are due to nonradiative deactivation induced by geometrical changes in the six-membered chelate rings of the ancillary ligands, which are supported by DFT study (*vide infra*), and intramolecular rotations in the excited state.[6a,6e,7c]

The complexes **1** and **2** in rigid media show strong orange emissions, and the red-shifted and increased emissions compared to those in fluid media (DMSO) result from restrictions of geometrical changes and of intramolecular rotations in the excited state. The emission spectra in poly(methyl methacrylate) (PMMA, 1 wt %) films at room temperature and in DMSO at 77 K show emission maxima at 596 and 582 nm for **1**, respectively, and 587 and 556 nm for **2**,

respectively (Fig. S1, ESI†). The quantum yields of **1** and **2** in PMMA films are 0.11 and 0.060, respectively. The large red-shifts from emissions in fluid media are found, although these emissions are derived from complexes themselves without intermolecular interactions. Based on the results, we assume that the complexes in rigid media emit from different triplet states, which are sustained by restrictions of geometrical changes in the excited state, from those in fluid media, and thus the emissions in rigid media probably attributed to $^3ML_{SB\text{-}COO(H)}CT$ character.

In the solid state, both complexes show red-orange emissions, and the emission spectra present broad bands centered at 610 and 606 nm for **1** and **2**, respectively (Fig. 2). The quantum yields of **1** and **2** are 0.046 and 0.015, respectively. The excitation spectrum of **1** in the solid state, which is monitored at λ_{em} = 610, shows a red-shifted band from that in solution state, monitored at 518 nm (Fig. 2A). In the case of **2**, a similar situation with that of **1** can be seen, in which the excitation spectra are monitored at 522 and 606 nm in solution and the solid state, respectively (Fig. 2B). The red-shifts in excitation bands indicate that the complexes in the solid state involving intermolecular interactions with neighboring complexes are excited. These observations indicate that the red-shifted and lowered emissions from ones in rigid media are caused by intermolecular interactions between complexes, and accordingly the emissions originate from metal-to-ligand-ligand charge transfer (^{3}MLLCT) state.[7c]

The emission spectra of **1** in DMSO/water mixtures were recorded with different water content (0 ~ 95%). As the fraction of water is increased, the solutions exhibit a clear Tyndall effect, indicating aggregation of **1**. In the solution with water fraction of 95%, aggregate of **1** shows an enhanced and red-shifted emission centered at 616 nm compared to that in solution state (Fig. 3). The excitation spectra show a decrease and increase in intensities at 381 and 413 nm, respectively, as an increase in water fraction (Fig. S2A, ESI†). The ^{1}H NMR spectrum in DMSO-d_6/D_2O mixed solvent exhibits sifted resonances from those in DMSO-d_6 alone (Fig. S2B, ESI†). These changes by an increase in water fraction suggest that the complexes in the aggregate state are involved in intermolecular interaction with neighboring complexes.

The increase in emission intensity is induced by restrictions of geometrical changes in the six-membered chelate ring of the ancillary ligand and of intramolecular rotations in the excited state.

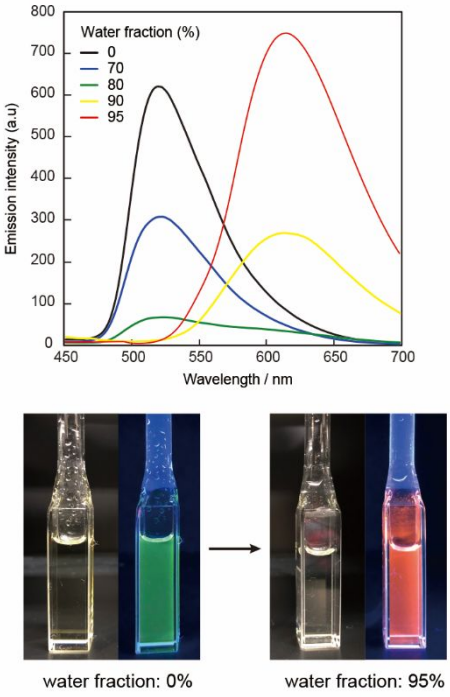

Fig. 3. Emission spectra of **1** in DMSO/water mixed solutions with different water fractions (0–95% v/v). Photos (left: under ambient light; right: under UV light irradiation (λ_{ex} = 365 nm)) of **1** in DMSO (water fraction of 0%) and DMSO/water mixed solution with water fraction of 95%.

Theoretical calculations

DFT and TD-DFT calculations for **1** and **2** in the ground (S_0) and excited triplet (T_1) states were performed.[16]

The optimized structures of **1** and **2** in the S_0 state have molecular structures that are similar to each other and those of previously reported Ir complexes containing anlinesalicylaldehyde Schiff base derivatives.[6a,7c] The $N{=}C_{(SB)}$ bond lengths (**1**: 1.308 Å; **2**: 1.305 Å) are typical for N=C double bonds. The $C_{(Ph–COO(H))}–N{=}C_{(SB)}–C_{(Ph\text{-}O)}–C–O$ atoms are nearly coplanar. The $C_{(Ph–COO(H))}$ atoms of **1** and **2** are located ca. 0.20 and 0.22 Å out of the $N{=}C_{(SB)}–C_{(Ph\text{-}O)}–C–O–$ planes (α, Fig. 4A), respectively, and the angles between the $C_{(Ph–COO(H))}–N$ direction and the $N{=}C_{(SB)}–C_{(Ph\text{-}O)}–C–O–$ plane (β, Fig. 4A) are ca. 8.1 and 8.7° for **1** and **2**, respectively. The dihedral angles between the phenyl ring of Ph–COO(H) and the $N{=}C_{(SB)}–C_{(Ph\text{-}O)}–C–O–$ plane are ca. 56.7 and 57.7° for **1** and **2**, respectively.

The dominant frontier molecular orbitals (MOs), the lowest unoccupied molecular orbitals (LUMOs) and the highest occupied molecular orbitals (HOMOs), of **1** and **2** are depicted in Fig. 5, and their energies and compositions are listed in Table 1. The LUMOs of **1** and **2** are located mainly over the ancillary ligand and the ppy ligands, respectively. Both LUMO+1 and LUMO+2 for **1** consist mainly of the π orbitals of the ppy ligands, and those of **2** are formed by the π orbitals of the salicylaldimine fragment and ppy ligands. The HOMOs of **1** and **2** have similar electron distributions, wherein the MOs consist mainly of the π orbitals of the salicylaldimine fragment and the dπ orbitals of the Ir centers. The electrons for HOMO−1 of **1** are located over the ppy ligands, Ir center, and salicylaldimine fragment, while those of **2** are distributed over

the ppy ligands, Ir center, and salicylaldimine moiety with distribution on the COO^- fragment.

The TD-DFT calculations for **1** and **2** revealed three intense transitions in the visible region originating from a combination of MLCT, LC, and ILCT transitions, as listed in Table 2. The calculated transition models agree well with the corresponding experimental data (Fig. 2). For **1**, the transitions at both 439 and 424 nm are derived from a combination of HOMO and HOMO−1 → LUMO transitions originating from $ML_{SB\text{-}COOH}CT$, $LC_{SB\text{-}COOH}$, and $IL_{SB\text{-}COOH}CT$, and that at 417 nm results from HOMO and HOMO−1 → LUMO+1 attributed to $ML_{ppy}CT$ transitions. The transitions for **2** at 424, 407, and 392 nm are derived mainly from HOMO and HOMO−1 → LUMO ($ML_{ppy}CT$ transition), HOMO → LUMO+1 and LUMO+2 ($ML_{ppy}CT$, $ML_{SB\text{-}COO}CT$, and $L_{SB\text{-}COOH}C$ transitions), and HOMO−1 → LUMO+1 and LUMO+2 ($ML_{ppy}CT$ and $ML_{SB\text{-}COO}CT$ transitions), respectively.

The optimized structures of **1** and **2** in the T_1 state show distortions of the chelate rings of ancillary ligands with a decrease in the double-bond character of the $N{=}C_{(SB)}$ bonds, as depicted in Figs. 4B and S3, ESI†. The calculated spin densities of both complexes are dominated by the cyclometalating ligands, Ir center, and ancillary ligands (Fig. 5B). The $N{-}C_{(SB)}$ bonds of both complexes (**1**: 1.386 Å; **2**: 1.404 Å) are extended by ca. 0.10 Å from those in the S_0 state. At the $Ir{-}N{=}C_{(SB)}{-}C_{(Ph\text{-}O)}{-}C{-}O$ chelate rings, the dihedral angles between the coordination plane, which comprises Ir, N, and O atoms, and the $N{=}C_{(SB)}{-}C_{(Ph\text{-}O)}{-}C{-}O$ plane vary from 9.7 and 11° for **1** and **2** in the S_0 state, respectively, to 37° and 40° for **1** and **2** in the T_1 state, respectively (Figs. 4B and S3, ESI†). The separations α and angles β for **1** and **2** are 0.68 Å and 29°, and 0.78 Å and 34°, respectively. These results support the low emission intensities observed experimentally in solution are caused by the geometrical changes in the chelate rings of the ancillary ligands as well as intramolecular rotations in the excited state.

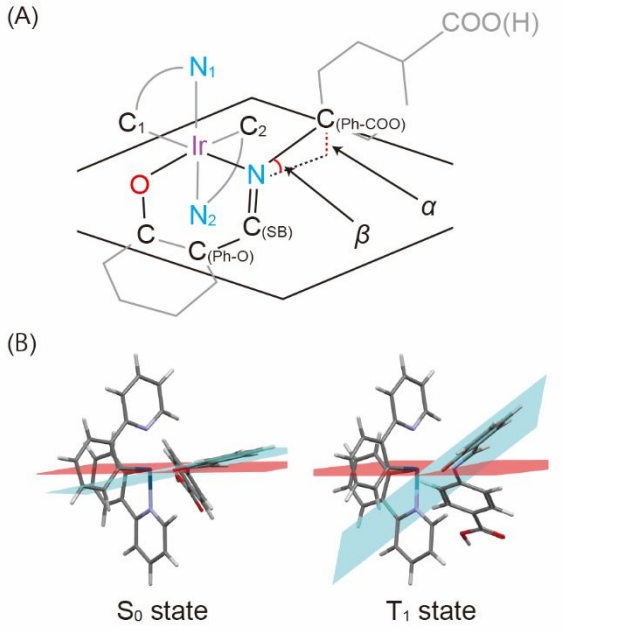

Fig. 4. (A) Separation between the $C_{(Ph\text{–}COO)}$ atom and the $N{=}C_{(SB)}{-}C_{(Ph\text{-}O)}{-}C{-}O{-}$ plane (α) and the angle between the $C_{(ph\text{-}COO)}{-}N$ direction and the $N{=}C_{(SB)}{-}C_{(Ph\text{-}O)}{-}C{-}O{-}$ plane (β). (B) Optimized structures of **1** in the S_0 (left) and T_1 (right) states. Red plane: coordination plane (Ir, N, O); blue plane: $N{=}C_{(SB)}{-}C_{(Ph\text{-}O)}{-}C{-}O$ plane.

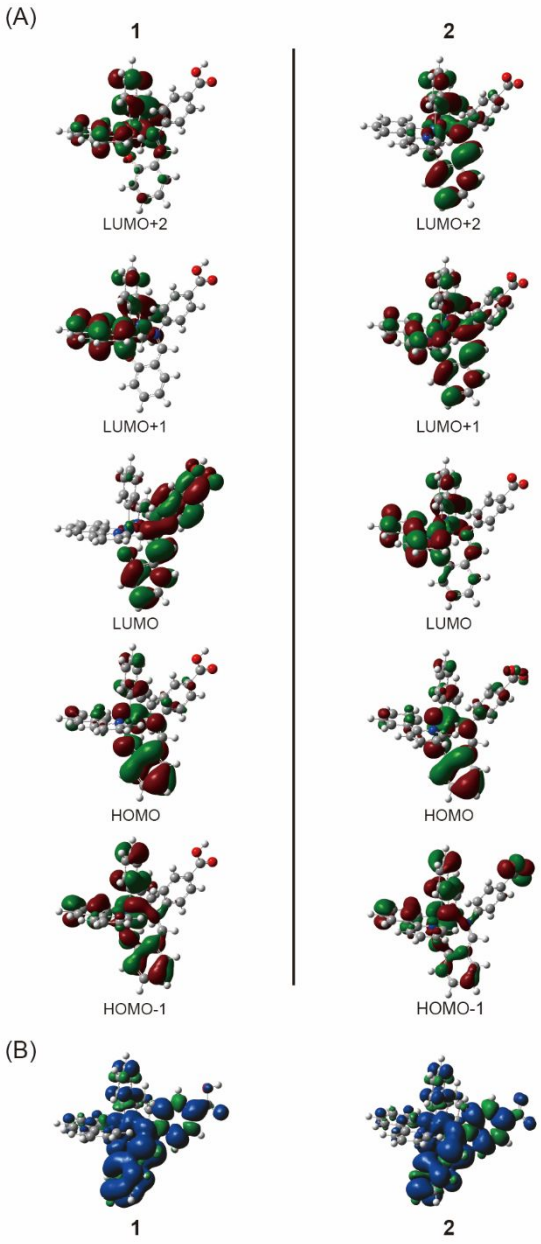

Fig. 5. (A) MOs for the optimized structures of **1** and **2** in the S_0 state. (B) Spin density distributions of **1** and **2** in the T_1 state.

Table 1. Calculated energy levels (eV) of selected MOs and their relative compositions (Ir: ppy: SB-COO(H)) for the optimized structures of **1** and **2** in the S_0 state.

	1	**2**
LUMO+2	−1.461, (6:87:7)	−1.368, (4:45:51)
LUMO+1	−1.533, (5:91:4)	−1.418, (3:59:38)
LUMO	−1.774, (2:7:91)	−1.480, (4:86:10)
HOMO	−5.202, (31:14:55)	−5.080, (28:12:60)
HOMO−1	−5.313, (46:33:21)	−5.220, (41:31:28)

Table 2. Calculated absorption maxima, transition energies (eV), oscillator strengths (f_{calcd}), and major transition contributions for the optimized structures of **1** and **2**.

	λ_{calcd} (nm)	E (ev)	f_{calcd}	major contribution
1	439	2.82	0.058	HOMO → LUMO (81%)
				HOMO−1 → LUMO (15%)
	424	2.93	0.072	HOMO−1 → LUMO (80%)
				HOMO → LUMO (16%)
	417	2.97	0.043	HOMO → LUMO+1 (53%)
				HOMO−1 → LUMO+1 (37%)
	404	3.07	0.009	HOMO → LUMO+1 (41%)
				HOMO−1 → LUMO+1 (40%)
				HOMO → LUMO+2 (17%)
	396	3.13	0.010	HOMO−1 → LUMO+2 (75%)
				HOMO−1 → LUMO+2 (18%)
2	424	2.92	0.039	HOMO → LUMO (66%)
				HOMO−1 → LUMO (27%)
	413	3.00	0.013	HOMO → LUMO+1 (49%)
				HOMO → LUMO+2 (15%)
				HOMO−1 → LUMO (14%)
				HOMO−1 → LUMO+1 (12%)
	407	3.05	0.074	HOMO → LUMO+2 (58%)
				HOMO → LUMO+1 (27%)
				HOMO−1 → LUMO+2 (12%)
	400	3.10	0.013	HOMO−1 → LUMO+1 (52%)
				HOMO−1 → LUMO+2 (16%)
	392	3.16	0.048	HOMO−1 → LUMO+2 (54%)
				HOMO−1 → LUMO+1 (19%)

pH-responsive AIEP of 2

The emission spectra of **2** recorded from aqueous solutions in the pH range of 8.7–1.8, where the concentration of the complex was kept at 2.0×10^{-5} mol/L, reveal the occurrence of AIEP at pH 4.7 (Fig. 6). Furthermore, strongly acidic conditions (pH ≤ 2.8) show decreased emission intensities owing to dissociation of the ancillary ligand from the $Ir(ppy)_2$ unit.

In basic and neutral pH solutions (pH ≥ 6.0), the complex exhibits weak emission comparable to that in DMSO. The emission spectrum recorded at pH 8.7 presents an emission band at 508 nm, which is a slightly different wavelength from that in DMSO (*vide supra*). At pH 7.2, 6.3, and 6.0, no apparent increase in intensity is found (Fig. 6A).

At pH 4.7, the complex exhibits AIEP with a bathochromic shift in emission color (Fig. 6). The solution shows a clear Tyndall effect, indicating the aggregated state of the complex. The emission spectrum presents a band at 618 nm, the intensity of which is increased ca. 50-fold compared to that at pH 7.2 (Fig. 6A). These observations reveal that protonation of the anionic complex **2** in aqueous solution leads to the formation and consequent aggregation of **1**, and the restricted geometrical change in the six-membered chelate ring of the ancillary ligand and the restricted intramolecular rotations in the excited state cause emission enhancement. Thus, H^+-responsive AIEP was achieved. The excitation spectrum at pH 4.7 shows a red-shifted band from that at pH 8.7 (Fig. S4, ESI†). The protonation and deprotonation cycle can be repeated many times (Fig. 6B), indicating a reversibility of the pH responsive ability.

Below pH 2.8, a decrease in emission intensity is observed, and the situation is caused by degradation of the luminescent aggregate **1** into the less luminescent $[\{Ir(ppy)_2\}_2(\mu\text{-}Cl)_2]$, 4-carboxylaniline, and salicylaldehyde. At pH 2.8, the emission intensity decreases compared to that at pH 4.7 without a shift in the band position. The solution at pH 1.8 presents an additional decrease in emission intensity from that at pH 2.8. The ^1H NMR spectrum of **1** in DMSO-d_6 in the presence of HCl shows a different pattern to that of **1** and HSBCOOH in DMSO-d_6 alone, but an identical pattern to those of HSB-COOH and $[\{Ir(ppy)_2\}_2(\mu\text{-}Cl)_2]$ in DMSO-d_6 in the presence of HCl (Fig. S5, ESI†). These results indicate that acidic conditions (pH < 4.7) lead to dissociation of the SB-$COOH^-$ ligand from the $Ir(ppy)_2$ fragment and subsequently hydrolysis of HSB-COOH to 4-carboxylaniline and salicylaldehyde. Furthermore, $Ir(ppy)_2^+$ forms the halogen-bridged Ir dimer $[\{Ir(ppy)_2\}_2(\mu\text{-}Cl)_2]$.[17]

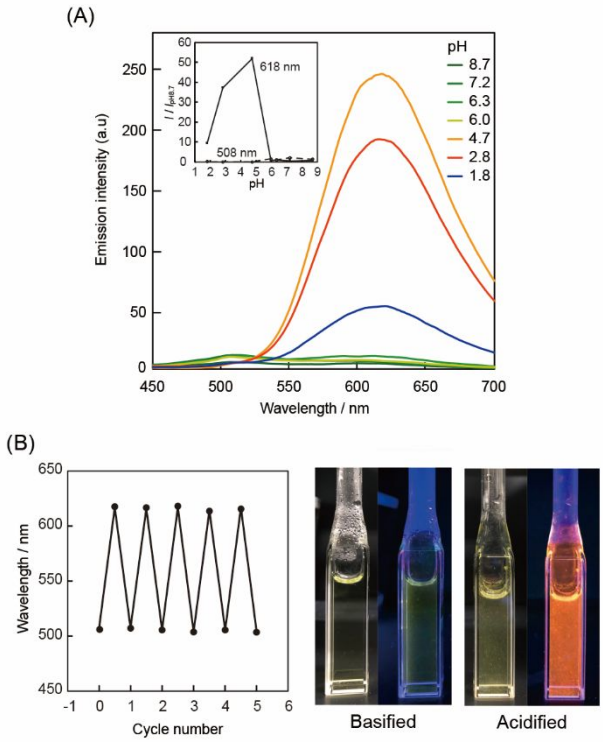

Fig. 6 (A) pH-dependent luminescence spectra of **2**; insert: changes in the emission intensity ($I/I_{pH8.7}$) at 508 nm (dashed line) and 618 nm (solid line). (B) Emission changes in the repeated cycles of adding NaOH(aq.) and after adding HCl(aq.). Photographs of **2** in aqueous solution under basic and acidic conditions (left: under ambient light; right: under UV light irradiation (λ_{ex} = 365 nm)).

Conclusions

In this work, we demonstrated H^+-responsive AIEP by the novel water-soluble monoanionic Ir(III) complex $Na[Ir(ppy)_2(SB\text{-}COO)]$. The emission spectra of $Na[Ir(ppy)_2(SB\text{-}COO)]$ recorded in aqueous solutions with pH values ranging 8.7–1.8 revealed the occurrence of H^+-induced AIEP at pH 4.7. The aggregation originates from the formation of the protonated species $Ir(ppy)_2(SB\text{-}COOH)$, which has poor solubility in aqueous solutions, and the enhanced emission is caused by the

restrictions of geometrical change in the six-membered chelate ring containing the ancillary ligand and of intramolecular rotations in the excited state.

Experimental

General procedures

The ancillary ligand HSB-COOH was synthesized by the method adopted by Alt with some modification.[14] The precursor dichlorido-bridged Ir dimer $[\{Ir(ppy)_2\}_2(\mu\text{-}Cl)_2]$ and complexes **1** were prepared by the method adopted by Davies[15] and Park[6a], respectively, with some modification. $IrCl_3{\cdot}3H_2O$ was purchased from Tanaka Kikinzoku Kogyo. All other reagents were purchased from commercial vendors and used without further purification. The DMSO used for measurement of UV-Vis and emission spectra was anhydrated over molecular sieves (3 Å) and deaerated by bubbling argon for at least 15 min prior to use. Other commercially available reagents were purchased and used without further purification. The ^1H and ^{13}C NMR spectra were recorded on a Bruker AVANCE-400 spectrometer in DMSO-d_6 with $(CH_3)_4Si$ (δ = 0) as an internal reference. The UV-Vis and emission spectra were recorded using JASCO V-530 and FP-6600 spectrometers, respectively. The luminescence quantum efficiencies were measured using a HAMAMATSU C9920-02 absolute photoluminescence quantum yield measurement system equipped with integrating sphere apparatus and a 150 W CW xenon light source. The luminescence lifetimes were recorded using a HAMAMATSU C11367-04 fluorescence lifetime measurement system with an LED laser at 365 nm excitation. Elemental analysis was performed using FISONS EA 1112 and EA 1108 instruments at the Comprehensive Analysis Center for Science, Saitama University, Japan.

Theoretical calculations

Quantum mechanical calculations were performed using the Gaussian 09W program suite.[16] Geometry optimizations for the ground state (S_0) and the excited triplet state (T_1) were performed using the B3LYP and unrestricted B3LYP (UB3LYP) levels, respectively, and were implemented in the Gaussian suite of the program.[18] The optimizations were followed by frequency calculations to verify that the obtained stationary points were the true energy minima. The 6-31G** basis set was used for all atoms except the Ir atom,[19] which was treated with the LANL2DZ basis set.[20] A polarized continuum model method was used to mimic the influence of the DMSO solvent in the calculations for complexes in the solution state, and this model was used during the optimization process and TD-DFT calculations. The Cartesian coordinates of the optimized structures are summarized in Tables S1–S4, ESI†. Selected bond lengths and structural parameters (α and β) of the optimized structures for 1 and 2 are given in Table S5. The optimized structures and frontier MOs were visualized using GaussView.

Syntheses and crystallizations.

[Ir(ppy)$_2$(SA-COOH)] (1).

The Ir(III) dichlorido-bridged dimer $[\{Ir^{III}(ppy)_2\}_2(\mu\text{-}Cl)_2]$ (0.21 g, 0.20 mmol), HSA-COOH (0.14 g, 0.60 mmol), NEt_3 (170 µL, 1.2 mmol) in MeOH (30 mL) were refluxed for 15 h. After cooling at room temperature, the suspension was filtered to obtain an orange powder, which was washed with MeOH, water, and diethyl ether; furthermore, the obtained powder was dried under vacuum. Yield: 0.12 g (39%). ^1H NMR (400 MHz, DMSO-d_6): δ = 12.7 (br, 1H), 8.91 (d, *J* = 5.0 Hz, 1H), 8.66 (d, *J* = 5.6 Hz, 1H), 8.26 (s, 1H), 8.15 (d, *J* = 8.0 Hz, 1H), 7.94-7.89 (m, 3H), 7.71 (d, *J* = 7.0 Hz, 1H), 7.42-7.38 (m, 1H), 7.34-7.30 (m, 4H), 7.22-7.16 (m, 2H), 6.79 (td, *J* = 6.5 Hz, 1.0 Hz, 1H), 6.61 (td, *J* = 6.3 Hz, 1.0 Hz, 1H), 6.48-6.38, (m, 3H), 6.33 (t, *J* = 6.8 Hz, 1H), 6.24 (d, *J* = 6.7 Hz, 2H), 6.03 (d, *J* = 7.0 Hz, 1H) 5.93 (d, *J* = 7.0 Hz, 1H). ^{13}C NMR (100 MHz, DMSO-d_6): δ = 167.7, 167.6, 166.7, 165.9, 161.8, 155.2, 152.0, 149.7, 147.4, 144.9, 144.3, 137.8, 136.3, 134.3, 132.5, 131.9, 128.6, 128.4, 126.7, 123.8, 123.6, 123.4, 122.8, 122.4, 121.3, 120.7, 119.4, 119.2, 118.6, 112.9. UV/Vis (2.6×10^{-5} mol/L, DMSO): λ_{max} (ε / M^{-1} cm^{-1}) = 453 (sh, 5800), 406 (9100), 345(sh, 11000). Anal. calcd. for $C_{36}H_{26}IrN_3O_3$: C, 58.37; H, 3.54; N, 5.67. Found: C, 58.26; H, 3.28; N, 5.51.

Na[Ir(ppy)$_2$(SA-COO)] (2).

$[Ir(ppy)_2(SA\text{-}COOH)]$ (**1**, 0.12 g, 0.20 mmol) in MeOH (30 mL) was deprotonated through the addition of a solution of NaOMe in MeOH (0.038 ml, 28%), and the reaction mixture was stirred at room temperature for 2 h. The solvent was removed under reduced pressure and the residual solid was recrystallized from MeOH solution by the addition of hexane. The obtained powder was filtered and dried under vacuum. Yield: 0.087 g (76%). ^1H NMR (400 MHz, DMSO-d_6): δ = 8.90 (d, *J* = 5.7 Hz, 1H), 8.67 (d, *J* = 5.7 Hz, 1H), 8.19 (s, 1H), 8.14 (d, *J* = 8.2 Hz, 1H), 7.92-7.88 (m, 3H), 7.69 (d, *J* = 7.8 Hz, 1H), 7.39-7.22 (m, 6H), 7.15 (t, *J* = 6.6 Hz, 1H), 6.78, (t, *J* = 6.5 Hz, 1H), 6.61 (t, *J* = 6.4 Hz, 1H), 6.46-6.36 (m, 3H), 6.31 (t, *J* = 7.7 Hz, 1H), 6.07 (d, *J* = 8.2 Hz, 2H), 6.03 (d, *J* = 7.5 Hz, 1H), 5.93 (d, *J* = 7.5 Hz, 1H). ^{13}C NMR (100 MHz, DMSO-d_6): δ = 169.3, 167.9, 167.4, 165.8, 161.8, 152.8, 152.7, 149.9, 149.5, 147.4, 144.9, 144.2, 137.6, 136.6, 136.3, 134.0, 132.4, 131.9, 128.3, 128.2, 123.8, 123.7, 123.2, 122.7, 121.9, 121.5, 120.8, 120.6, 119.4, 119.2, 118.5, 112.7. UV/Vis (2.1×10^{-5} mol/L, DMSO): λ_{max} (ε) = 458 (sh, 6000), 404 (12000), 344(sh, 14000).

ACKNOWLEDGMENT

This study was supported by the Global Science Campus program, Japan Science and Technology Agency (JST), through the High-grade Global Education Program for Sciences, Saitama University. We thank Prof. Masa-aki Haga (Department of Applied Chemistry, Faculty of Science and Engineering, Chuo University) for the emission lifetime measurements.

References

1 (a) C. Adachi, M. A. Baldo, S. R. Forrest and M. E. Thompson, *Appl. Phys. Lett.,* 2000, **77**, 904–906. (b) M. A. Baldo, M. E.

Thompson and S. R. Forrest, *Nature*, 2000, **403**, 750–753. (c) S. Lamansky, P. Djurovich, D. Murphy, F. Abdel-Razzaq, H.-E. Lee, C. Adachi, P. E. Burrows, S. R. Forrest and M. E. Thompson, *J. Am. Chem. Soc.*, 2001, **123**, 4304−4312. (d) M. K. Nazeeruddin, R. Humphry-Baker, D. Berner, S. Rivier, L. Zuppirol and, M. Graetzel, *J. Am. Chem. Soc.*, 2003, **125**, 8790−8797. (e) A. Tsuboyama, H. Iwawaki, M. Furugori, T. Mukaide, J. Kamatani, S. Igawa, T. Moriyama, S. Miura, T. Takiguchi, S. Okada, M. Hoshino and K. Ueno, *J. Am. Chem. Soc.*, 2003, **125**, 12971–12979. (f) M. S. Lowry, W. R. Hudson, R. A. Pascal Jr. and S. Bernhard, *J. Am. Chem. Soc.*, 2004, **126**, 14129−14135. (g) S. Obara, M. Itabashi, F. Okuda, S. Tamaki, Y. Tanabe, Y. Ishii, K. Nozaki and M. Haga, *Inorg. Chem.*, 2006, **45**, 8907–8921. (h) E. Baranoff, S. Suàrez, P. Bugnon, C. Barolo, R. Buscaino, R. Scopelliti, L. Zuppiroli, M. Graetzel and M. K. Nazeeruddin, *Inorg. Chem.*, 2008, **47**, 6575–6577. (i) W.-Y. Wong and C.-L. Ho, *Coord. Chem. Rev.,* 2009, **253**, 1709−1758. (j) S. Ladouceur and E. Zysman-Colman, *Eur. J. Inorg. Chem.,* 2013, 2985–3007. (k) A. F. Henwood and E. Zysman-Colman, *Chem. Commun.*, 2017, **53**, 807–826.

2 (a) P. Alam, G. Kaur, C. Climent, S. Pasha, D. Casanova, P. Alemany, A. R. Choudhury and I. R. Laskar, *Dalton Trans.*, 2014, **43**, 16431−16440. (b) S. Sharma, H. Kim, Y. H. Lee, T. Kim, Y. S. Lee and M. H. Lee, *Inorg. Chem.,* 2014, **53**, 8672–8680. (c) H.-T. Cao, L. Ding, G.-G. Shan, H.-Z. Sun, Y. Wu and Z.-M. Su, *Dalton Trans.,* 2015, **44**, 19997–20003. (d) W. Wang, Z. Mao, M. Wang, L.-J. Liu, D. W. J. Kwong, C.-H. Leung, D.-L. Ma, *Chem. Commun.,* 2016, **52**, 3611−3614.

3 (a) Y. Yang, Q. Zhao, W. Feng and F. Li, *Chem. Rev.,* 2013, ***113***, 192−270. (b) Y. Chen, L. Qiao, B. Yu, G. Li, C. Liu, L. Ji and H. Chao, *Chem. Commun.,* 2013, ***49***, 11095–11097.

4 Y. Kawamura, J. Brooks, J. J. Brown, H. Sasabe and C. Adachi, *Phys. Rev. Lett.,* 2006, **96**, 017404.

5 (a) J. Luo, Z. Xie, J. W. Y. Lam, L. Cheng, H. Chen, C. Qiu, H. S. Kwok, X. Zhan, Y. Liu, D. Zhu and B. Z. Tang, *Chem. Commun.,* 2001, 1740–1741. (b) C. H. Shin, J. O. Huh, M. H. Lee and Y. Do, *Dalton. Trans.,* 2009, 6476−6479. (c) H. Wu, T. Yang, Q. Zhao, J. Zhou, C. Li and F. Li, *Dalton Trans.,* 2011, **40**, 1969–1976. (d) Q. Zhao, L. Li, F. Li, M. Yu, Z. Liu, T. Yi and C. Huang, *Chem. Commun.,* 2008, 685−687. (e) P. Alam, M. Karanam, A. R. Choudhury and I. R. Laskar, *Dalton. trans.,* 2012. ***42***. 9276–9279. (f) X. Zhang, Z. Chi, Y. Zhang, S. Liu and J. Xu, *J. Mater. Chem. C,* 2013, **1**, 3376–3390. (g) Y. Wu, H.-Z. Sun, H.-T. Cao, H.-B. Li, G.-G. Shan, Y.-A. Duan, Y. Geng, Z.-M. Su and Y. Li, *Chem. Commun.,* 2014, **50**, 10986–10989. (h) G. Li, Y. Wu, G. Shan, W. Che, D. Zhu, B. Song, L. Yan, Z. Su and M. R. Bryce, *Chem. Commun.,* 2014, **50**, 6977–6980. (i) J. Mei, N. L. C. Leung, R. T. K. Kwok, J. W. Y. Lam and B. Z. Tang. *Chem. Rev.,* 2015, **115**, 11718−11940. (j) G. Li, W. Guan, S. Du, D. Zhu, G. Shan, X. Zhu, L. Yan, Z. Su, M. R. Bryce and A. P. Monkman, *Chem. Commun.,* 2015, **51**, 16924–16927. (k) Y. Jiang, G. Li, W. Che, Y. Liu, B. Xu, G. Shan, D. Zhu, Z. Su and M. R. Bryce, *Chem. Commun.,* 2017, **53**, 3022–3025.

6 (a) Y. You, H. S. Huh, K. S. Kim, S. W. Lee, D. Kim and S. Y. Park, *Chem. Commun.,* 2008, 3998–4000. (b) G.-G. Shan, D.-X. Zhu, H.-B. Li, P. Li, Z.-M. Su and Y. Liao, *Dalton Trans.,* 2011, **40**, 2947–2953. (c) G.-G. Shan, L.-Y. Zhang, H.-B. Li, S. Wang, D.-X. Zhu, P. Li, C.-C. Wang, Z.-M. Su and Y. Liao, *Dalton Trans.,* 2012, **41**, 523–530. (d) G.-G. Shan, H.-B. Li, H.-Z. Sun, D.-X. Zhu, H.-T. Cao and Z.-M. Su, *J. Mater. Chem. C,* 2013, **1**, 1440–1449. (e) Y. Jiang, G. Li, D. Zhu, Z. Su and M. R. Bryce, *J. Mater. Chem. C,* 2017, **5**, 12189–12189.

7 (a) M. Ghedini, A. Golemme, I. Aiello, N. Godbert, R. Termine, A. Crispini, M. La Deda, F. Lelj, M. Amati and S. Belviso, *J. Mater. Chem.,* 2011, **21**, 13434−13444. (b) S. Liu, H. Sun, Y. Ma, S. Ye, X. Liu, X. Zhou, X. Mou, L. Wang, Q. Zhao and W. Huang, *J. Mater. Chem.,* 2012, **22**, 22167−22173. (c) A. J. Howarth, R. Patia, D. L. Davies, F. Lelj, M. O. Wolf and K. Singh, *Eur. J. Inorg. Chem.,* 2014, 3657–3664.

8 K. Huang, H. Wu, M. Shi, F. Li, T. Yi and C. Huang, *Chem. Commun.* 2009, 1243−1245.

9 (a) S. Modi, M. G. Swetha, D. Goswami, G. D. Gupta, S. Mayor and Y. Krishnan, *Nat. Nanotechnol.*, 2009, **4**, 325–330. (b) J. Han and K. Burgess, *Chem. Rev.,* 2010, **110**, 2709–2728. (c) K. Zhou, Y. Wang, X. Huang, K. Luby-Phelps, B. D. Sumer and J. Gao, *Angew. Chem. Int. Ed.,* 2011, **50**, 6109 –6114. (d) M. Yang, Y. Song, M. Zhang, S. Lin, Z. Hao, Y. Liang, D. Zhang and P. R. Chen, *Angew. Chem., Int. Ed.,* 2012, **51**, 7674–7679. (e) R. C. Somers, R. M. Lanning, P. T. Snee, A. B. Greytak, R. K. Jain, M. G. Bawendi and D. G. Nocera, *Chem. Sci.,* 2012, **3**, 2980–2985. (f) M. Liu, M. Hu, Q. Jiang, Z. Lu, Y. Huang, Y. Tan and Q. Jiang, *RSC Adv.,* 2015, **5**, 15778–15783.

10 (a) P. Song, X. Chen, Y. Xiang, L. Huang, Z. Zhou, R. Wei and A. Tong, *J. Mater. Chem.,* 2011, **21**, 13470–13475. (b) Q. Feng, Y. Li, L. Wang, C. Li, J. Wang, Y. Liu, K. Li and H. Hou. *Chem. Commun*., 2016, **52**, 3123-3126. (c) N. Lin, X. Chen, S. Yan, H. Wang, Z. Lu, X. Xia, M. Liang, Y.-L. Wu, L. Zheng, Q. Cao and Z. Ding, *RSC Adv.,* 2016, **6**, 25416–25419. (d) Y. Yuan, C.-J. Zhang, R. T. K. Kwok, D. Mao, B. Z. Tang and B. Liu, B. *Chem. Sci.* 2017, **8**, 2723–2728.

11 (a) A. Nakagawa, Y. Hisamatsu, S. Moromizato, M. Kohno and S. Aoki, *Inorg. Chem.,* 2014, **53**, 409−422. (b) A. Kando, Y. Hisamatsu, H. Ohwada, T. Itoh, S. Moromizato, M. Kohno and S. Aoki, *Inorg. Chem.,* 2015, **54**, 5342-5357. (c) P. Alam, G. Kaur, S. Chakraborty, A. R. Choudhury and I. R. Laskar, *Dalton Trans.,* 2015, **44**, 6581−6592.

12 P. Alam, G. Kaur, A. Sarmah, R. K. Roy, A. R. Choudhury and I. R. Laskar, *Organometallics,* 2015, **34**, 4480−4490.

13 D. Chao and Y. Zhang, *Sens. Actuators, B,* 2017, **245**, 599−604.

14 (a) H. G. Alt, K. J. Schneider, *Jor. J. Chem.,* 2008, **3**, 11−32. (b)S. K. Shrivastavaa, P. Srivastavaa, T.V.R. Upendraa, P. N. Tripathi and S. K. Sinha, *Bioorg. Med. Chem.,* 2017, **25**, 1471−1480.

15 D. L. Davies, M. P. Lowe, K. S. Ryder, K. Singh and S. Singh, *Dalton Trans.,* 2011, **40**, 1028−1030.

16 M. J. Frisch, G. W. Trucks, H. B. Schlegel, G. E. Scuseria, M. A. Robb, J. R. Cheeseman, G. Scalmani, V. Barone, B. Mennucci, G. A. Petersson, H. Nakatsuji, M. Caricato, X. Li, H. P. Hratchian, A. F. Izmaylov, J. Bloino, G. Zheng, J. L. Sonnenberg, M. Hada, M. Ehara, K. Toyota, R. Fukuda, J. Hasegawa, M. Ishida, T. Nakajima, Y. Honda, O. Kitao, H. Nakai, T. Vreven, J. A. Montgomery Jr., J. E. Peralta, F. Ogliaro, M. Bearpark, J. J. Heyd, E. Brothers, K. N. Kudin, V. N. Staroverov, R. Kobayashi, J. Normand, K. Raghavachari, A. Rendell, J. C. Burant, S. S. Iyengar, J. Tomasi, M. Cossi, N. Rega, J. M. Millam, M. Klene, J. E. Knox, J. B. Cross, V. Bakken, C. Adamo, J. Jaramillo, R. Gomperts, R. E. Stratmann, O. Yazyev, A. J. Austin, R. Cammi, C. Pomelli, J. W. Ochterski, R. L. Martin, K. Morokuma, V. G. Zakrzewski, G. A. Voth, P. Salvador, J. J. Dannenberg, S. Dapprich, A. D. Daniels, O. Farkas, J. B. Foresman, J. V. Ortiz, J. Cioslowski and D. J. Fox, *Gaussian 09, Revision C. 01*, Gaussian, Inc., Wallingford CT, 2009.

17 (a) D. R. Whang, Y. You, W.-S. Chae, J. Heo, S. Kim and S. Y. Park, *Langmuir,* 2012, **28**, 15433−15437. (b) E. Baranoff, B. F. E. Curchod, J. Frey, R. Scopelliti, F. Kessler, I. Tavernelli, U. Rothlisberger, M. Grätzel and Md. K. Nazeeruddin, *Inorg. Chem.,* 2012, **51**, 215−224.

18 (a) C. T. Lee, W. T. Yang and R. G. Parr, *Phys. Rev. B,* 1988, **37**, 785−789. (b) A. D. Becke, *J. Chem. Phys.,* 1993, **98**, 5648−5652.

19 M. M. Francl, W. J. Pietro, W. J. Hehre, J. S. Binkley, M. S. Gordon, D. J. Defrees and J. A. Pople, *J. Chem. Phys.,* 1982, **77**, 3654−3665.

20 P. J. Hay and W. R. Wadt, *J. Chem. Phys.,* 1985, **82**, 299−310.

The novel Na[Ir(ppy)$_2$(SB-COO)] (Hppy = phenylpyridine; HSB-COOH = 4-carboxylanilinesalicylaldehyde Schiff base) in aqueous solution showed pH-responsive aggregation-induced enhanced phosphorescence (AIEP) by the formation of the protonated species [Ir(ppy)$_2$(SB-COOH)].